Comparison of Beam Theory and Finite-Element Analysis With In Vivo Bone Strain Data From the Alligator Cranium

KEITH A. METZGER,[1]* WILLIAM J.T. DANIEL,[2] AND CALLUM F. ROSS[3]

[1]Department of Anatomical Sciences, Stony Brook University, Stony Brook, New York
[2]School of Engineering, University of Queensland, Queensland, Australia
[3]Organismal Biology and Anatomy, University of Chicago, Chicago, Illinois

ABSTRACT

The mechanical behavior of the vertebrate skull is often modeled using free-body analysis of simple geometric structures and, more recently, finite-element (FE) analysis. In this study, we compare experimentally collected in vivo bone strain orientations and magnitudes from the cranium of the American alligator with those extrapolated from a beam model and extracted from an FE model. The strain magnitudes predicted from beam and FE skull models bear little similarity to relative and absolute strain magnitudes recorded during in vivo biting experiments. However, quantitative differences between principal strain orientations extracted from the FE skull model and recorded during the in vivo experiments were smaller, and both generally matched expectations from the beam model. The differences in strain magnitude between the data sets may be attributable to the level of resolution of the models, the material properties used in the FE model, and the loading conditions (i.e., external forces and constraints). This study indicates that FE models and modeling of skulls as simple engineering structures may give a preliminary idea of how these structures are loaded, but whenever possible, modeling results should be verified with either in vitro or preferably in vivo testing, especially if precise knowledge of strain magnitudes is desired.   © 2005 Wiley-Liss, Inc.

Key words: bone strain; finite-element analysis; skull biomechanics; alligator; feeding

Biomechanical models of the vertebrate skull often invoke simple beam, plate, or cylindrical structures as geometric models to make predictions regarding in vivo bone strain patterns (Preuschoft et al., 1983, 1986; Thomason and Russell, 1986; Russell and Thomason, 1993; Ross and Hylander, 1996; Ravosa et al., 2000; Ross, 2001; Rafferty et al., 2003). Although this approach has proven to be useful in some cases, in vivo bone strain values often diverge from expectations based on simple geometric models. For example, although bone strain orientation patterns in the skull of the strepsirrhine primate *Otolemur* match those predicted for a simple cylinder under torsion (Ravosa et al., 2000; Ross, 2001), those in the circumorbital regions of anthropoid primates *Macaca* and *Aotus* do not (Hylander et al., 1991; Ross and Hylander, 1996; Ross, 2001). The reason for these differing results is not clear. It

might be the case that the anthropoid skull actually is twisting, but the complexity of its geometry and material properties cause the strain patterns to diverge from those of a simple cylinder. Alternately, the skull might be behaving very similarly to a simple cylinder subjected to some unknown loading regime. Without additional infor-

*Correspondence to: Keith A. Metzger, Department of Anatomical Sciences, Stony Brook University, HSC T-8, Stony Brook, NY 11794. Fax: 631-444-3947. E-mail: kmetzger@ic.sunysb.edu

mation, it is impossible to choose between these two possibilities.

Finite-element analysis (FEA) provides a method for choosing between these two alternatives. FEA of the macaque skull, validated by in vivo bone strain data (Strait et al., 2003, this issue; Ross et al., 2005, this issue), suggests that during unilateral biting and mastication, the macaque skull is not twisted, but instead is subjected to a complex deformation of the circumorbital region similar to that reported from in vitro studies of *Homo* and *Gorilla* (Endo, 1966).

Crocodilians are another example where simple beam models have been used to infer function and interpret design of the skull. For example, despite the fact that modern crocodilians have diverged from tubular morphology in being notably platyrostral (dorsoventrally flattened snouts), it has been suggested that the in vivo behavior of the crocodilian rostrum during biting can be understood by modeling it as a cylindrical structure that is subjected to bending and twisting moments during unilateral and bilateral biting (Ferguson, 1981; Preuschoft et al., 1986; Busbey, 1995). Moreover, a number of morphological changes characterizing crocodilian evolution are hypothesized to be linked to increasing the mechanical resistance of the crocodilian cranium to these bending and torsional moments. These include fusion of the medial palatal plates, and posterior extension of the bony palate as well as the development of broad overlapping scarf joints between cranial elements (Langston, 1973; Busbey, 1995; Cleuren and De Vree, 2000).

Two of us (K.A.M. and C.F.R.) have been collecting in vivo bone strain data to test these hypotheses regarding the behavior of the crocodilian snout during biting. However, as with the primate studies, when the in vivo data diverge from the strict predictions of beam theory, it is difficult to determine whether this is because the loading regime is not as predicted, or the geometry invalidates predictions based on simple geometric structures.

This article examines whether FEA can be used to alleviate these problems by deriving predictions for in vivo bone strain from a finite-element model (FEM) that more closely approximates skull geometry than a simple geometric structure does. Here, we make predictions regarding in vivo bone strain in the alligator (*Alligator mississippiensis*) rostrum using simple beam mechanics theory, modeling the snout as a bending and twisting beam with a solid ellipsoid cross-section. Next, we use FEA to make predictions regarding bone strain patterns at selected sites on the alligator snout. Finally, we report the strain patterns recorded from three in vivo experiments and compare these with the simple beam and FEA predictions.

Previously, validation studies have compared experimental strain results with those derived from FEA. However, these are typically conducted using either skeletal elements with a relatively simple geometric structure (Gross et al., 1997, 2002; Kotha et al., 2004) or in vitro strain data (Gupta et al., 2004). This study represents one of the first validation studies of a geometrically complex skeletal structure using in vivo data collected under naturalistic conditions (Strait et al., 2003, 2005, this issue).

MATERIALS AND METHODS
Application of Beam Theory

In order to predict deformation patterns in the crocodilian skull from standard beam theory, reference was made
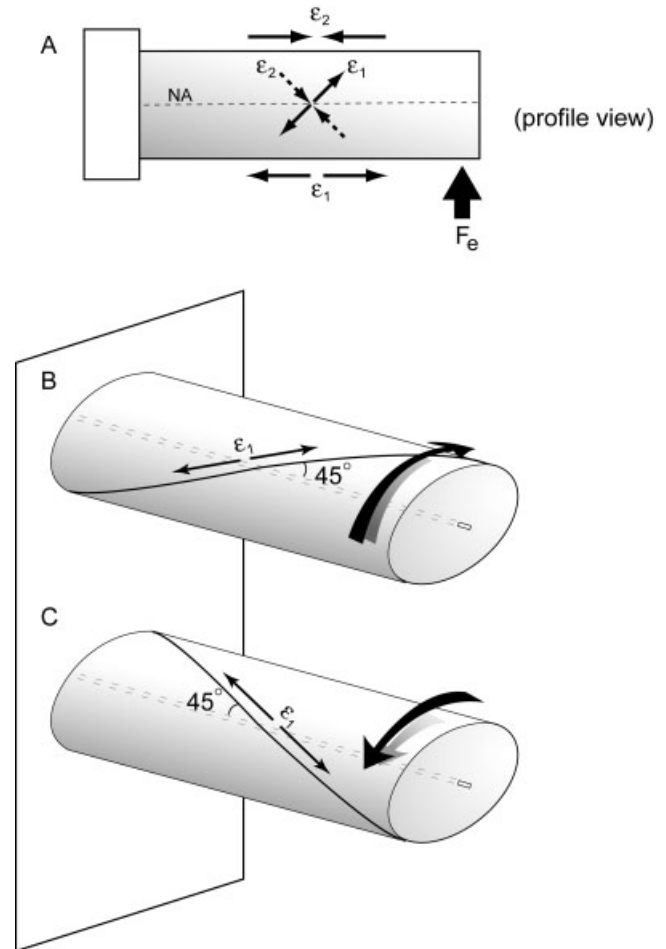

Fig. 1. Orientations of principal strains on the surfaces of a bending and a twisting ellipsoid beam. **A:** Profile view of an ellipsoid beam cantilevered at one end and subjected to a bending moment caused by an external force (F_e). The upper surface of the beam is subjected to compression (ϵ_2) along the long axis of the beam and tension (ϵ_1) along the long axis on the bottom surface. Normal strains as they cross the neutral axis (NA) are at 45° angles to the long axis, and they are smaller than the normal strains at the dorsal and ventral surfaces. **B** and **C:** Orientation of maximum principal strain (ϵ_1) on the surface of an ellipsoid beam subjected to a twisting moment by external force (curved arrow). Compressive strain (ϵ_1) is of equal magnitude and oriented perpendicular to the tensile strain.

to an engineering textbook, *Mechanics of Materials*, by Hibbeler (2000), as well as to Biewener (1992). For estimation of strain orientations, the skull was analogized to a cantilevered ellipsoid beam (to simulate platyrostry) fixed at its posterior end, to which an upwardly directed external force was applied at various places (i.e., bite points; Fig. 1). Specific predictions regarding principal strain orientations were generated using Hibbeler's (2000) discussions of torsion (p. 177–253), bending (p. 255–361), and combined loadings (p. 409–438). In the beam model, no attempt was made to simulate the local or global effects of jaw musculature.

To predict strain in the skull due to bending caused by specific bites, bending stress at a point in a beam section was calculated using the formula: $\sigma = My/I$, where M is

the bending moment, y is the perpendicular distance from the neutral axis to the point of interest (strain gauge location), and I is the second moment of area of the section of interest (Hibbeler, 2000). Then, strains were calculated from these values by dividing by the same Young's (elastic) modulus as was used for the FEM (10 GPa). Bending moments (Nm) varied by bite point and were the same as used for loading the FEM. The second moments of area (I) of sections at which gauges were placed were calculated from coronal section scans published by the University of Texas Digimorph project (Brochu et al., 1998). At each of these sections, maximum width and height of the skull were measured, scaled to the size of the experimental animals using equivalent measurements and an assumption of isometry, and used to calculate second moment of area, I, using the formula for a solid ellipse. Perpendicular distance from the neutral axis to gauge location was simply the distance from the strain gauge location to the neutral axis of bending, which was assumed to pass horizontally through the section centroid. Strain values were expected to be significantly lower than functional strains reported from in vivo studies, since the second moment of area was calculated based on a solid beam rather than a hollow structure. Although shear strains from torsion in an ellipsoid beam were not quantified, predictions were made based on engineering principles discussed below.

Finite-Element Analysis

Finite-element model construction. The geometric properties of the skull model were obtained using publicly available CT scans of a subadult American alligator skull (*Alligator mississippiensis*; Texas Memorial Museum M-983; skull length, 30.2 cm), published on the Internet by the University of Texas Digimorph project (www.digimorph.org). Coordinates were read from CT sections, and node points placed at these coordinates on each section were manually joined to create finite elements. Because CT sections were extracted from MPEG data and were of relatively low-resolution, there is some uncertainty in estimation of between-section coordinates. The 3D model was then scaled down to the actual length of the animals used during the in vivo experiments assuming geometric similarity and using head length, biquadrate length, and tooth row length as scaling factors. Strand v6.16 was used for model construction and implementation (G+D Computing, Sydney, Australia).

Approximately 2,400 shell elements were used to represent the cranium (the mandible was not included in this FEM), with 1,453 nodes (Fig. 2). Although this is a relatively coarse model, more elements were not justified due to the nature of the coordinate data. Because shell elements assume a linear variation of in-plane displacements through the thickness of the element, this model is of a more limited accuracy in thicker regions of the cranium (e.g., quadrates, basicranium), but it is appropriate for the regions focused on in this study (i.e., rostrum, skull roof). Each shell element is a flat surface, representing the midsurface of the bone, and each is of constant thickness. In addition to in-plane deformation, shell elements can bend and twist out-of-plane. Use of shells places two significant limitations on geometric modeling. First, artificial stress concentrations can occur when a faceted surface replaces a doubly curved surface. Second, sudden geometric changes are present in the model that may be more gradual in
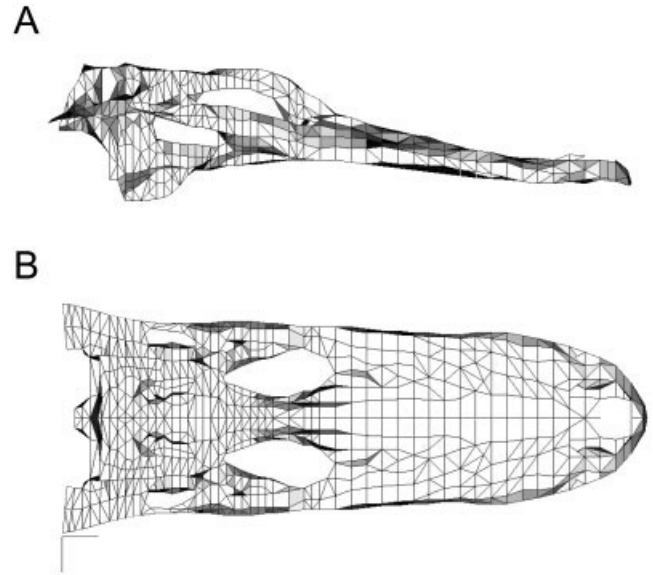

Fig. 2. Lateral (**A**) and dorsal (**B**) views of the finite-element model of *Alligator mississippiensis*. The model was comprised of 2,400 shell elements and 1,453 nodes.

reality. More details of model construction can be found in Daniel and McHenry (2001).

Material properties. The elastic properties used in this model were a Young's (elastic) modulus of 10 GPa (the stress/strain ratio for uniaxial loading) and a Poisson's ratio of 0.4 (Daniel and McHenry, 2001). Potential orthotropic properties of the alligator cranium were not included in this model because there has not been adequate material testing performed, although this will be included when such data become available. However, for this study, after an isotropic solution was obtained, the FEM was rerun with orthotropic properties using a transverse elastic modulus of only 5 (instead of 10) GPa along a fiber. Fiber directions were assigned to agree with the directions of principal tension or compression (whichever had the greater stress) read from the results of the isotropic model. Although the results of this comparison will not be discussed in this study, in general, the use of orthotropic properties results in higher stresses (Daniel and McHenry, 2001).

Model loading. Muscle loads were applied as described in Daniel and McHenry (2001) using muscle physiological cross-sectional areas taken from Sinclair and Alexander (1987) and Busbey (1989) and assuming bilateral, simultaneous, and maximal contraction of all adductor muscles. Muscle forces were distributed over nodes positioned approximately at attachment areas. The model was constrained with spring supports placed at the jaw joints. It is worth noting that although the jaw joints have been fixed in the model, indirect in vivo evidence suggests that both tensile and compressive loading may be present within the joint (Metzger et al., 2003).

To simulate biting at different points, the model was loaded at each of 11 bite locations (Fig. 3B; anterior midline; right: anterior, anterior/middle, middle, middle/pos-
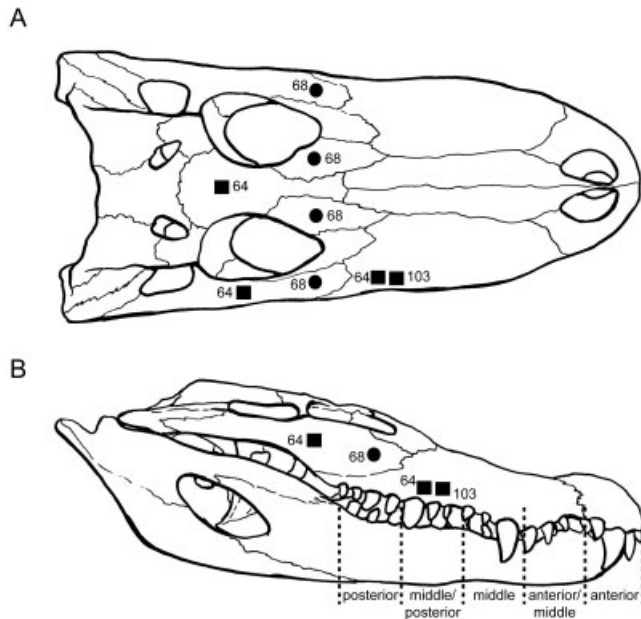
Fig. 3. Dorsal (**A**) and lateral (**B**) views of the skull of *Alligator mississippiensis*. Squares represent location of delta rosette strain gauges and circles represent rectangular rosettes. Numbers adjacent to gauge sites refer to experiment number. On the lateral view, the right lower tooth row is divided into the bite point regions used for this study (anterior, anterior/middle, middle, middle/posterior, posterior). The left tooth row was divided in the same way and anterior midline bites were also considered separately.

TABLE 1. Experimental summary including type of strain gauge and strain gauge positions

Experiment number	Gauge type	Animal number	Gauge location
64	Delta	1	Midline frontal, right posterior jugal, right posterior maxilla
68	Rectangular	1	Right anterior jugal, right prefrontal, left prefrontal, left anterior jugal
103	Delta	2	Right maxilla

Animals were maintained by the Stony Brook University Division of Laboratory Animal Resources in accordance with the National Institutes of Health Guidelines for the Care and Use of Laboratory Animals. All experimental procedures were approved by the Stony Brook Institutional Animal Care and Use Committee (IACUC 2002-1112).

Data collection. Stacked delta rosette strain gauges (SA-06-030WY-120; Micromeasurements, Raleigh, NC) or rectangular rosette strain gauges (FRA 1-11-1L; Texas Measurements, College Station, TX) were wired, insulated, and gas-sterilized using procedures described previously (Ross, 2001). All surgeries were performed with the animal under 2% isofluorane anesthesia administered in oxygen through an intubation tube. Following induction of anesthesia, 1 cm squares of skin overlying the gauge sites were removed, the periosteum was elevated, the bone degreased with chloroform, and the gauge bonded to the surface of the bone using cyanoacrylate adhesive. Gauges were placed in various locations, including the maxilla above the tooth row (two), anterior jugal (one), posterior jugal (two), prefrontal (two), and midline frontal (one) bones (Fig. 3A, Table 1). After the gauges were attached, the wires were glued and sutured to the skin overlying the skull and then run through a plastic tube secured to the back of the animal with self-adhesive VetWrap and surgical tape.

Animals were allowed to recover from surgery (at least 2 hr), and then strains were recorded while the animal bit on a custom-built bite force recording device at different locations along the tooth row. The bite device consists of two 6 mm steel bite plates attached to a piezoelectric force transducer located behind a pivot point [modeled after Herrel et al. (2001)]. The force transducer (type 9301B; Kistler, Switzerland) was connected to a charge amplifier, and bite force data were recorded synchronously with the strain data. The steel bite plates were covered with several layers of surgical tape, and the upper layer was replaced after each bite so that the position of the bite on the bite plate could be accurately recorded using the tooth impression on the tape. Bite point locations were assigned to 11 regions: an anterior region at the front of the tooth row on the midline, and anterior, anterior/middle, middle, middle/posterior, and posterior regions on each side (Fig. 3B). Biting side/location along the tooth row and the presence of any unusual activity (shake, attempted twisting) were recorded on a data sheet.

All strain data, transmitted as voltage changes, were conditioned and amplified on Vishay 2100 bridge amplifi-

terior, posterior; left: same as right). Bite force was distributed evenly along the bite region, because point loading resulted in unstable strain orientations, and because in vivo loading was distributed along the width of the bite force device. A total of 22 model loading experiments was conducted, representing all bite locations for which data were available from the three in vivo experiments. Bite force used to load the model at a given bite location was the average in vivo value recorded during all bites at that location during a given experiment. For example, during experiment 64, the average recorded bite force from the nine left middle bites was 116 N; this was used as the bite force applied to the FEM at the left middle bite point. After models were run, principal strain orientations and magnitudes were extracted from the elements located at the experimental gauge sites. All model loadings were conducted by W.J.T.D. without any a priori knowledge of the in vivo strain magnitudes or orientations.

Strain Gauge Recording and Analysis

Subjects. Two subadult American alligators (*Alligator mississippiensis*; head length, 12.3 and 17.5 cm) were used for 3 separate experiments (experiments 64, 68, and 103). Animals were housed separately in large plastic tanks with both a wet and a dry area on a 12-hr light/dark cycle and were fed three times per week on mice, chicken, and fish ad libitum. The environmental temperature ranged from 28°C during the day to 20°C at night, with a heater to keep water at a relatively constant temperature (27°C).

ers. Data were acquired at 1 KHz through a National Instruments DAQ board run by MiDAS data acquisition software package (Xcitex, Cambridge, MA).

Data analysis. Strain data were filtered and processed in IGOR Pro 4.0 (WaveMetrics, Lake Oswego, OR) using custom-written software. The strain data were converted to microstrain ($10^{-6} \epsilon$, $\Delta L/L$) using calibration files made during the recording sessions. The following variables were then calculated and are reported below: magnitude of maximum (ϵ_1) and minimum principal strains (ϵ_2) and maximum shear strain (γ_{max}) (Hibbeler, 2000). Maximum principal strain (ϵ_1) is usually the largest tensile strain value, while the minimum principal strain is usually the largest compressive strain value (ϵ_2). $\epsilon_1 - \epsilon_2$ is equal to the maximum shear strain, or γ_{max}. Additionally, the orientation of the maximum (tensile) principal strain relative to the sagittal axis of the skull and the ratio of maximum to minimum principal strains ($|\epsilon_1/\epsilon_2|$) were calculated and are reported. All data were split into 11 groups based on the 11 tooth row regions into which the bite locations were assigned, as described above. Statistical tests discussed below were conducted using SPSS v11.5 (SPSS, Chicago, IL).

Comparison of Beam Model, FEM, and In Vivo-Derived Data

Strain magnitudes. The strain magnitudes predicted for the beam model under bending are oriented normal to the parasagittal plane (long axis of the snout), whereas the strains calculated for the FEM and in vivo data are principal strains and therefore these are not necessarily directly comparable to each other. In order to make the FEA and in vivo data comparable to beam strains, the component of strain parallel to the parasagittal plane at each gauge site was calculated from the principal strains using the formula:

$$\frac{\epsilon_1 + \epsilon_2}{2} + \frac{\epsilon_1 - \epsilon_2}{2} \cos2\alpha + \frac{\gamma_{12}}{2} \sin2\alpha$$

where ϵ_1 and ϵ_2 are maximum and minimum principal strains and α is the angle between ϵ_1 and the mid-sagittal plane (Hibbeler, 2000: p. 491). When ϵ_1 and ϵ_2 are principal strains, as is the case here, shear strain γ_{12} equals 0, and the term $\frac{\gamma_{12}}{2}\sin2\alpha$ is ignored.

Because absolute strain magnitudes from the beam model were expected to be lower than FEM and in vivo strains (for reasons described above), an analysis on ranks (Friedman's test) was performed on the data collected during loading at each bite point. This test evaluates the null hypothesis that rank order of strain values at the recording sites does not differ across treatments (i.e., beam, FEM, in vivo). This test was performed on the data recorded or extracted during loading/biting at each bite point. For each bite point, a three-way test (beam, FEA, in vivo) and three pairwise tests (beam vs. FEA, beam vs. in vivo, FEA vs. in vivo) were performed. The test output is a Kendall's W-statistic, which ranges from 0 (no agreement in rank) to 1 (complete agreement), and a significance value.

Principal strain orientations. Orientation of maximum principal (ϵ_1) strain was compared across the three
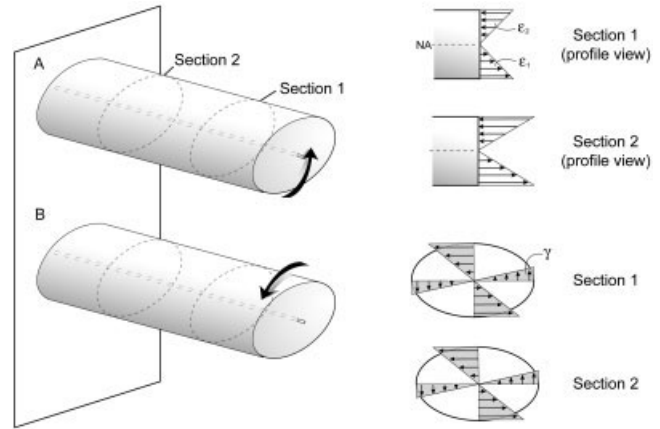

Fig. 4. Strain distributions at different sections of an ellipsoid beam loaded in bending (**A**) and twisting (**B**). ϵ_1, tension; ϵ_2, compression; γ, shear due to torsion.

data sets. For the beam model, inferences based on bending and torsion of an ellipsoid member (Figs. 1 and 4) allow comparison to the FEA and in vivo data. The strain orientations in the FEA and in vivo data sets were compared by calculating the difference between the two values for each bite point/strain gauge (Tables 6–8). The value used for the in vivo data was the average orientation recorded for all bites during biting in each region.

RESULTS
Predictions Based on Beam Theory

Beam theory strain magnitudes. Calculated bending strains in the beam were always tensile at the sites representing jugal gauge positions (range, 6.0–33.8 $\mu\epsilon$) and compressive at all other gauge positions (range, -20.3 to -114.8 $\mu\epsilon$), regardless of load point location. Strains were typically highest at positions representing the dorsoventral positions of the frontal, prefrontal, and maxillary gauges (Table 2).

Beam theory strain orientations. Biting at the rostral end of the tooth row exerts primarily shear and bending moments on the snout, whereas unilateral biting at the posterior end of the tooth row exerts predominantly torsional moments. Only exact midline bites (or bilateral bites with equal right and left side bite force magnitudes) will produce a pure loading regime (bending and shear without torsion), and even posterior tooth row bites generate shear and bending moments in more caudal sections. The relative importance of bending and torsion presumably varies with bite position, from predominantly bending during anterior bites to predominantly torsion during posterior bites.

In an ellipsoid beam subjected to upwardly directed bending, the patterns of strain orientation are those illustrated in Figure 1A (i.e., compression along the long axis of the top of the beam, and tension along the long axis of the bottom). Strain orientations on the side of the beam depend on the location relative to the bending axis (of neutrality), and they will curve along the side of the beam, crossing the neutral axis at a 45° angle.

In an ellipsoid beam under torsion, the faces of elements oriented parallel to the beam's twisting axis are subjected

TABLE 2. Calculated second moments of area and strain (με) for sites of interest when the skull is modeled as a ellipsoid beam in pure dorsal bending

Gauge location	Bite location		Strain (με)
Frontal	Midline		−64.7
	Left	a	−26.1
		m	−82.7
I = 136,719 mm⁴		m/p	−97.1
		p	−60.5
	Right	a	−47.7
		a/m	−89.1
		m	−103.9
		m/p	−57.4
		p	−39.5
Right jugal (64)	Midline		18.1
	Left	a	7.1
		m	20.5
I = 64,967 mm⁴		m/p	22.7
		p	9.9
	Right	a	13.1
		a/m	23.5
		m	25.8
		m/p	13.4
		p	6.5
Right maxilla	Midline		−100.6
	Left	a	−36.3
		m	−53.5
	Right	a	−66.4
I = 6,993 mm⁴		a/m	−96.4
		m	−67.2
Right jugal (68)	Midline		6.5
	Left	a	8.5
		a/m	6.8
I = 44,173 mm⁴		m	21.1
		m/p	21.3
		p	6.3
	Right	a	15.5
		m	33.8
		p	6.0
		p	6.5
Right prefrontal	Midline		−22.0
	Left	a	−29.0
		a/m	−23.1
I = 44,173 mm⁴		m	−72.0
		m/p	−72.3
		p	−21.6
	Right	a	−52.6
		m	−114.8
		p	−20.3
Left prefrontal	Midline		−22.0
	Left	a	−29.0
		a/m	−23.1
I = 44,173 mm⁴		m	−72.0
		m/p	−72.3
		p	−21.6
	Right	a	−52.6
		m	−114.8
		p	−20.3
Left jugal	Midline		6.5
	Left	a	8.5
		a/m	6.8
I = 44,173 mm⁴		m	21.1
		m/p	21.3
		p	6.3
	Right	a	15.5
		m	33.8
		p	6.0

to pure shear. Hence, maximum principal strain orientations are oriented in a helical pattern, with tension oriented at 45° to the twisting axis (Fig. 1B), reversing in direction with changes in twisting direction. This orientation will hold true regardless of where the beam is sampled.

When the snout is modeled as an ellipsoid beam, as the bite point moves posteriorly along the tooth row from an anterior midline bite to a posterior unilateral bite, maximum principal strain angle on the dorsal surface should rotate clockwise: from an orientation perpendicular to the long axis of the skull (the theoretical twisting axis) toward a 45° orientation relative to the long axis. This represents a transition in loading regime from one of dorsal bending at anterior bite points to increasing torsion at more posterior ones.

FEA Results

FEM strain magnitudes. Full descriptive statistics derived from the finite-element model are given in Tables 3–5. The within-gauge means of maximum (ϵ_1) principal strain ranged from 55 to 230 με, and the grand mean across all bite points was 120 με. For minimum (ϵ_2) principal strain, within-gauge means ranged from −226 to −378 με with a grand mean of −296 με. t-tests on principal strain data recorded from each site under all loading regimes revealed significant differences between working and balancing side minimum principal strain magnitudes only at the right jugal and right prefrontal sites ($P < 0.05$). All other working-balancing side comparisons were not significant.

Model-derived $|(\epsilon_1/\epsilon_2)|$ ratios are also reported in Tables 3–5. In the majority of cases, side-averaged $|(\epsilon_1/\epsilon_2)|$ ratios indicate that compressive strain is predominant over tensile strain (i.e., the ratios are less than 1.0). Tensile strain is only greater than compressive at the frontal site during middle bites (simulating experiment 64; Table 3), at the right jugal sites during middle/posterior and posterior bites (simulating experiment 64; Table 3), and at the prefrontal sites during contralateral posterior bites (simulating experiment 68; Table 4).

FEM principal (ϵ_1) strain orientations. Descriptive statistics for model-derived ϵ_1 orientations are listed in Tables 6–8 and are displayed graphically in Figures 5–7. All angles are listed relative to the sagittal plane of the skull, with negative angles rotated clockwise and positive angles rotated counterclockwise. ϵ_2 orientations are not listed as they are by definition orthogonal (rotated 90°) to ϵ_1 orientations.

For midline (anterior) bites, ϵ_1 is oriented approximately in the coronal plane, averaging only 12° rotation from this plane across all gauges (Fig. 5). During unilateral bites, strain orientations vary between biting sides, but exhibit minimal variation among bite points within a side (Figs. 6 and 7). During right unilateral bites, ϵ_1 is almost always oriented between 45° and 90° at the frontal, right jugal (experiment 64 location), right maxilla (experiment 64 location), and right prefrontal sites (Fig. 6, Tables 6 and 7). At the right jugal (experiment 68 location), left prefrontal, left jugal, and right maxilla sites (experiment 103 location), ϵ_1 orientations are higher than 90° and range up to 135°. Slightly less variability is observed in ϵ_1 orientations during left side bites, both among sites for a particular bite point, and within a site across bite

TABLE 3. Descriptive statistics for principal (ϵ_1 and ϵ_2) and $|(\epsilon_1/\epsilon_2)|$ strain magnitudes for model and in vivo analysis of experiment 64*

Gauge location	Bite location		n	ϵ_1				ϵ_2				$|(\epsilon_1/\epsilon_2)|$ ratio		
				Model	Mean	SD	Max	Model	Mean	SD	Max	Model	Mean	SD
Frontal	Midline		2	204	408	695	900	−272	−114	139	−212	0.75	0.61	6.87
	Left	a	4	76	234	97	370	−112	−80	33	−127	0.68	2.93	0.32
		m	9	250	810	404	1388	−430	−266	106	−391	0.58	2.89	0.48
		m/p	7	264	942	205	1189	−510	−327	53	−386	0.52	2.86	0.20
		p	7	363	642	144	791	−457	−250	38	−307	0.79	2.54	0.21
	All left		27		716	346			−250	103			2.80	0.35
	Right	a	2	139	286	40	315	−206	−94	11	−102	0.67	3.03	0.08
		a/m	4	299	669	394	1059	−467	−189	74	−262	0.64	3.30	0.79
		m	11	314	808	297	1161	−540	−249	81	−319	1.26	3.19	0.36
		m/p	7	156	597	201	857	−302	−212	49	−283	0.52	2.74	0.44
		p	9	237	299	92	430	−298	−134	31	−167	0.80	2.19	0.30
	All right		33		576	314			−193	78			2.83	0.59
	All bites		60		631	342			−216	96			2.70	1.18
Right jugal	Midline		2	68	5	172	126	−131	−115	152	−223	0.52	7.08	10.82
	Left	a	4	64	56	8	64	−354	−105	21	−136	0.18	0.54	0.08
		m	9	52	311	156	486	−90	−343	176	−529	0.58	0.92	0.10
		m/p	7	122	375	75	447	−102	−488	69	−543	1.20	0.76	0.06
		p	7	119	256	62	350	−73	−351	67	−456	1.63	0.73	0.08
	All left		27		275	142			−347	161			0.77	0.15
	Right	a	2	100	102	20	115	−122	−235	16	−247	0.82	0.43	0.05
		a/m	4	−133	508	235	752	−188	−916	480	−1,401	0.71	0.57	0.04
		m	11	259	1,164	484	1,887	−585	−1,873	768	−3,087	0.44	0.62	0.04
		m/p	7	61	1,368	353	1,811	−480	−2,286	618	−3,041	0.13	0.60	0.03
		p	9	17	1,004	215	1,178	−71	−1,526	479	−2,183	0.24	0.69	0.14
	All right		33		1,020	482			−1,651	798			0.62	0.10
	All bites		60		663	663			−1,033	888			0.44	1.96
Right maxilla	Midline		2	68	66	316	290	−130	−306	372	−569	0.52	1.61	2.99
	Left	a	4	64	61	30	99	−136	−110	57	−187	0.47	0.55	0.04
		m	9	215	163	94	295	−355	−300	173	−543	0.61	0.53	0.07
		m/p	7	122	175	44	231	−439	−315	91	−431	0.28	0.56	0.03
		p	7	201	108	34	161	−329	−173	60	−262	0.61	0.63	0.03
	All left		27		137	73			−243	137			0.57	0.06
	Right	a	2	80	146	3	149	−163	−293	0	−293	0.49	0.50	0.01
		a/m	4	183	557	352	916	−378	−956	659	−1,637	0.48	0.61	0.05
		m	11	−151	1,173	548	2,122	−543	−1,399	558	−2,148	0.28	0.83	0.10
		m/p	7	181	911	462	1,689	−614	−1,013	525	−1,932	0.29	0.90	0.04
		p	9	68	213	134	495	−276	−245	139	−526	0.25	0.85	0.08
	All right		33		719	570			−882	653			0.80	0.13
	All bites		60		444	511			−585	580			0.62	0.58

*For Tables 3–8, n refers to in vivo sample size only.

points (Fig. 7). At the frontal, right jugal (experiment 64, 68 locations), right maxilla (experiment 64, 103 locations), and left prefrontal sites, ϵ_1 orientations range from 90° to 120°. At the right prefrontal and left jugal sites, this value is slightly less than 90°, ranging from 56° to 80°. There is no apparent difference in variability of principal strain orientation across sites when data are grouped by simulated bite point location.

In Vivo Results

Potential problems with in vivo data collection. Strain magnitudes (γ_{max}, ϵ_1, and ϵ_2) and orientations from the left prefrontal gauge are highly irregular compared to the other in vivo results from these experiments. Strain magnitudes are significantly higher than at most other gauge sites and are notably higher than magnitudes from the right prefrontal, which was located in the same position but on the opposite side of the skull. Additionally, during biting at several bite point locations (e.g., midline, right anterior, right middle, right posterior; Figs. 5 and 6), ϵ_1 orientations at this gauge site are highly divergent from strain orientations of adjacent sites and sites along the same coronal plane. Although the strain gauge was properly attached throughout the experiment, because of these anomalies, results from this gauge are generally not included in this discussion.

Shear strain magnitudes. Full descriptive statistics of the maximum shear strain recorded from all strain gauges and all bite locations are given in Tables 9–11. The within-gauge means of maximum shear strain (γ_{max}) ranged from 631 to 1,907 µε, and the grand mean for all bite points was 1,350 µε. Although strain gauges were usually located at or behind the rear of the tooth row, shear strain values during posterior bites are not typically the highest seen, and in most gauge sites, a trend of increasing and then decreasing shear strain along the tooth row (anterior to posterior) is evident, with mean γ_{max} highest during biting at the middle or middle/posterior bite positions. Mean γ_{max} values vary broadly across gauge sites (range, 161–3,833 µε) and within gauge sites with variation in bite point. For all but one gauge site (left prefrontal gauge, experiment 68), working side bites (i.e., bites ipsilateral to the gauge) have the highest γ_{max}. In

TABLE 4. Descriptive statistics for principal (ϵ_1 and ϵ_2) and $|(\epsilon_1/\epsilon_2)|$ strain magnitudes for model and in vivo analysis of experiment 68*

Gauge location	Bite location		n	ϵ_1 Model	Mean	SD	Max	ϵ_2 Model	Mean	SD	Max	$|(\epsilon_1/\epsilon_2)|$ ratio Model	Mean	SD
Right jugal	Midline		10	13	333	317	969	−95	−716	749	−2,308	0.14	0.55	0.17
	Left	a	4	80	267	273	673	−102	−493	636	−1,415	0.78	1.04	0.80
		a/m	3	21	471	321	698	−33	−939	683	−1,431	0.64	0.55	0.11
		m	16	128	283	246	838	−137	−555	463	−1,465	0.93	0.54	0.16
		m/p	13	60	274	185	577	−97	−600	420	−1,229	0.62	0.49	0.18
		p	7	34	353	129	468	−145	−856	340	−1,207	0.24	0.42	0.05
	All left		43		303	217			−639	462			0.55	0.30
	Right	a	5	−71	472	209	698	−239	−1,262	651	−2,075	0.30	0.39	0.05
		m	20	106	945	187	1,474	−869	−2,044	518	−2,636	0.12	0.52	0.36
		m/p	1		676		676		−466		−466		1.45	
		p	10	537	828	379	1,238	−1,231	−980	386	−1,444	0.44	0.88	0.29
	All right		36		839	296			−1,596	713			0.63	0.38
	All bites		89		548	370			−1,075	757			0.59	0.34
Right prefrontal	Midline		10	37	251	217	712	−73	−559	640	−2,119	0.51	0.55	0.12
	Left	a	4	48	146	80	249	−102	−323	308	−765	0.47	0.58	0.19
		a/m	3	40	193	114	299	−49	−490	324	−704	0.82	0.46	0.16
		m	10 (6)	4	31 (97)	61 (32)	169	−62	−201 (−339)	−143 (−250)	−622	0.07	0.15 (0.34)	0.09 (0.11)
		m/p	11 (2)	3	166 (24)	161 (14)	398	−30	−370 (−101)	283 (81)	−762	0.10	0.36 (0.45)	0.16 (0.50)
		p	7	134	260	153	445	−126	−504	212	−705	1.06	0.45	0.19
	All left		43		134	133			−339	251			0.35	0.21
	Right	a	5	203	279	106	398	−359	−890	485	−1,478	0.57	0.36	0.12
		m	17 (3)	314	398 (31)	120 (33)	592	−603	−1,800 (−537)	−480 (−138)	−2,268	0.52	0.23 (0.05)	0.09 (0.05)
		m/p	1		34		34		−212		−212		0.16	
		p	6 (4)	271	82 (38)	61 (14)	183	−596	−597 (−232)	−92 (−141)	−682	0.45	0.15 (0.20)	0.11 (0.11)
	All right		36		248	186			−1,150	747			0.22	0.12
	All bites		89		186	168			−709	670			0.29	0.19
Left prefrontal	Midline		10	36	708	402		−73	−388	259	−1,091	0.49	1.90	0.60
	Left	a	4	112	517	161	698	−198	−221	131	−410	0.57	2.61	0.68
		a/m	3	79	713	274	927	−142	−538	447	−1,031	0.56	1.78	0.82
		m	16	197	340	318	1,214	−378	−346	268	−863	0.52	1.17	0.54
		m/p	13	175	279	161	556	−360	−724	645	−1,807	0.49	0.70	0.55
		p	7	287	377	135	504	−632	−987	471	−1,337	0.45	0.48	0.29
	All left		43		370	255			−566	504			1.09	0.79
	Right	a	5	86	1,005	350	1,269	−184	−868	320	−1,167	0.47	1.16	0.06
		m	16 (4)	6	1,751 (863)	222 (61)	1,996	−98	−2,085 (−2,166)	359 (428)	−2,561	0.06	0.86 (0.43)	0.15 (0.14)
		m/p	1		432		432		−1,075		−1,075		0.40	
		p	10	126	590	241	914	−112	−1,725	679	−2,530	1.13	0.34	0.03
	All right		36		1,190	575			−1,797	632			0.70	0.32
	All bites		89		743	593			−1,127	835			0.91	0.65
Left jugal	Midline		10	13	312	332	988	−95	−649	711		0.14	0.50	0.04
	Left	a	4	−39	361	427	999	−132	−768	985	−2,238	0.30	0.52	0.05
		a/m	3	9	677	464	1,014	−137	−1,499	1,087	−2,293	0.07	0.49	0.07
		m	10 (6)	67	431 (346)	334 (235)	1,020	−545	−1,029 (−313)	712 (137)	−2,264	0.12	0.42 (1.08)	0.09 (0.34)
		m/p	11 (2)	167	874 (188)	640 (192)	2,095	−646	−860 (−377)	507 (390)	−1,486	0.26	1.19 (0.51)	0.29 (0.02)
		p	7	570	1,678	586	2,253	−1,305	−1,140	334	−1,401	0.44	1.45	0.19
	All left		43		760	662			−882	658			0.90	0.45
	Right	a	5	146	176	128	389	−185	−323	272	−785	0.79	0.59	0.08
		m	20	204	457	130	652	−218	−861	256	−1,213	0.94	0.54	0.04
		m/p	1		429		429		−1,004		−1,004		0.43	
		p	10	32	312	103	431	−136	−675	240	−984	0.24	0.47	0.02
	All right		36		377	156			−739	309			0.52	0.06
	All bites		89		586	533			−817	530			0.73	0.38

*When two values are listed, there are two loading regimes present as indicated by principal strain orientations (secondary in parentheses). The regime with less bites in it is considered secondary.

TABLE 5. Descriptive statistics for principal (ϵ_1 and ϵ_2) and $|(\epsilon_1/\epsilon_2)|$ strain magnitudes for model and in vivo analysis of experiment 103

Gauge location	Bite location		n	ϵ_1 Model	Mean	SD	Max	ϵ_2 Model	Mean	SD	Max	$|(\epsilon_1/\epsilon_2)|$ ratio Model	Mean	SD
Right maxilla	Left	m	6	121	129	36	193	−353	−196	70	−326	0.34	0.67	0.04
		p	5	173	119	62	214	−284	−136	68	−156	0.61	0.86	0.04
	All left		11		124	47	214		−169	73	−326		0.76	0.11
	Right	a/m	4 (2)	−130	1,256 (1,758)	286 (66)	1,805	−202	−1,126 (−1,291)	254 (108)	−1,371	0.64	1.12 (1.36)	0.01 (0.06)
		m	2		1,955	388	2,230		−1,671	477	−2,009		1.18	0.11
		p	5		2,032	123	2,158		−1,911	91	−2,002		1.06	0.03
	All right		13		1,739	400			−1,537	408			1.14	0.11
	All bites		24		999	872			−910	758			0.97	0.23

TABLE 6. Descriptive statistics for maximum principal (ϵ_1) strain orientation values for model and in vivo analysis of experiment 64

| Gauge location | Bite location | | n | ϵ_1 angle relative to sagittal | | | |
				Difference	Model	Mean	SD
Frontal	Midline		2	21	90	111	16
	Left	a	4	3	105	102	2
		m	9	2	105	103	2
		m/p	7	1	104	105	1
		p	7	1	103	104	1
	All left		27	2	104	105	
	Right	a	2	12	75	87	1
		a/m	4	10	75	85	1
		m	11	10	75	85	2
		m/p	7	7	76	83	1
		p	9	5	78	83	1
	All right		33	8	76	85	
	All bites		60	7	89	95	
Right jugal	Midline		2	10	93	103	11
	Left	a	4	27	125	98	5
		m	9	8	118	110	5
		m/p	7	1	112	111	1
		p	7	0	111	111	2
	All left		27	9	112	107	
	Right	a	2	31	78	47	1
		a/m	4	46	85	39	1
		m	11	44	81	37	1
		m/p	7	46	80	34	2
		p	9	27	56	29	1
	All right		33	39	76	37	
	All bites		60	24	94	72	
Right maxilla	Midline		2	2	63	65	0
	Left	a	4	47	118	71	6
		m	9	38	118	80	4
		m/p	7	35	118	83	3
		p	7	29	117	88	2
	All left		27	37	118	81	
	Right	a	2	21	69	48	0
		a/m	4	46	72	26	2
		m	11	89	60	151	21
		m/p	7	52	79	131	4
		p	9	41	87	128	2
	All right		33	50	73	97	
	All bites		60	44	93	90	

nonmidline gauges (all except the frontal gauge), mean γ_{max} on the working side is on average 3.84 times greater than on the balancing side (range, 0.29–11.21).

Principal strain magnitudes. Full descriptive statistics of the in vivo principal strains are given in Tables 3–5. The within-gauge means of maximum (ϵ_1) principal strain ranged from 186 to 999 $\mu\epsilon$, and the grand mean for all bite points was 557 $\mu\epsilon$. For minimum (ϵ_2) principal strain, within-gauge means ranged from -216 to $-1,127$ $\mu\epsilon$, with a grand mean of -827 $\mu\epsilon$. Except in the left prefrontal gauge, mean ϵ_1 and ϵ_2 are greater on the working side than on the balancing side [mean working side/balancing side principal (ϵ_1 and ϵ_2) strain ratio for all gauges, 4.39; range, 0.31–14.0]. However, unpaired t-tests reveal few statistically significant differences between working and balancing side ϵ_1 and ϵ_2 (ϵ_1: right jugal WS > BS, $P < 0.01$; ϵ_2: right jugal, left prefrontal WS > BS, $P < 0.05$). Mean ϵ_1 recorded during biting across all bite points ranges from 186 (right prefrontal) to 999 $\mu\epsilon$ (right maxilla;

experiment 103), and mean ϵ_2 for all bite locations ranges from -216 (frontal) to $-1,175$ $\mu\epsilon$ (left prefrontal).

Descriptive statistics of the $|(\epsilon_1/\epsilon_2)|$ ratios are given in Tables 3–5. Values above 1 indicate higher tensile strains, and values below 1 indicate higher compressive strains. Overall, compressive strain exceeds tensile strain, although this pattern was reversed in the frontal gauge, and in the left prefrontal and maxillary (experiment 103) gauges, tension and compression are roughly equal. Unpaired sample t-tests reveal that for one of seven gauge sites, the mean $|(\epsilon_1/\epsilon_2)|$ ratio of all bite locations is significantly greater on the working side than on the balancing side (maxilla; experiment 64; $P < 0.05$).

Principal (ϵ_1) strain orientations. Descriptive statistics for ϵ_1 orientation are listed in Tables 6–8 and are also illustrated in Figures 5–7. Angle conventions are the same as described for the model-derived data. Strain orientations for the left prefrontal gauge are omitted from the following description.

TABLE 7. Descriptive statistics for maximum principal (ϵ_1) strain orientation values for model and in vivo analysis of experiment 68

Gauge location	Bite location		n	ϵ_1 angle relative to sagittal			
				Difference	Model	Mean	SD
Right jugal	Midline		10	21	100	79	7
	Left	a	4	25	95	70	17
		a/m	3	11	94	83	8
		m	16	8	91	83	11
		m/p	13	6	93	87	13
		p	7	22	104	82	3
	All left		43	14	95	81	
	Right	a	5	55	135	80	2
		m	20	39	106	67	20
		p	10	85	109	14	16
	All right		36	63	117	54	
	All bites		89	31	103	72	
Right prefrontal	Midline		10	1	75	−106	6
	Left	a	4	5	80	85	5
		a/m	3	36	56	92	5
		m	10 (6)	66	81	15 (47)	13 (7)
		m/p	11 (2)	58	77	19 (102)	17 (21)
		p	7	90	76	166	3
	All left		43	51	74	114	
	Right	a	5	11	75	64	1
		m	17 (3)	31	70	101 (21)	2 (5)
		p	6 (4)	47	60	13 (91)	2 (7)
	All right		36	30	68	64	
	All bites		89	38	72	96	
Left prefrontal	Midline		10	68	106	38	11
	Left	a	4	44	105	61	14
		a/m	3	27	107	80	17
		m	16	32	110	78	42
		m/p	13	46	113	159	47
		p	7	55	120	175	12
	All left		43	41	111	111	
	Right	a	5	79	100	21	2
		m	20	86	99	13	5
		p	10	61	104	165	4
	All right		36	75	101	66	
	All bites		89	55	107	88	
Left jugal	Midline		10	43	80	123	3
	Left	a	4	47	75	122	3
		a/m	3	51	75	126	6
		m	10 (6)	56	74	130 (16)	8 (16)
		m/p	11 (2)	55	72	127 (20)	9 (5)
		p	7	48	71	23	3
	All left		43	51	73	90	
	Right	a	5	40	85	125	5
		m	20	31	89	120	3
		p	10	46	77	123	3
	All right		36	39	84	123	
	All bites		89	46	78	109	

During midline bites (Fig. 5), maximum tensile strain at all sites is roughly oriented in the coronal plane; ϵ_1 averages 19° rotation (in either direction) from this plane. ϵ_1 orientations during unilateral bites are less consistent across all gauges than midline bites. Notable exceptions to this are the ϵ_1 orientations at the frontal gauge, which are extremely consistent across bite locations (95° ± 11°), almost exactly parallel with the coronal plane. In the other gauges, ϵ_1 orientations during anterior and anterior/middle bites are less variable among the gauge sites than during more posterior bites.

During right side bites, mean ϵ_1 orientations have a high degree of variability, especially at gauge locations near the bite point (Fig. 6). When all gauge sites are considered together for a given right side bite point, the range of strain orientations at any given site varies from 59° to 89°. Within-gauge variability for different right side bite locations is even more extreme, ranging from 3° to 88° and averaging 54°.

Mean ϵ_1 orientations during left side bites are generally more consistent than on the right side (Fig. 7). With only a few exceptions, maximum principal strain orientations

TABLE 8. Descriptive statistics for maximum principal (ϵ_1) strain orientation values for model and in vivo analysis of experiment 103

Gauge location	Bite location		n	ϵ_1 angle relative to sagittal			
				Difference	Model	Mean	SD
Right maxilla	Left	m	6	13	116	103	3
		m/p	5	2	106	104	2
	All left		11	8	111	104	
	Right	a/m	4 (2)	44	129	85 (3)	1 (6)
		m	2			170	19
		p	5			157	1
	All right		13	44	129	137	
	All bites		24	19	117	124	
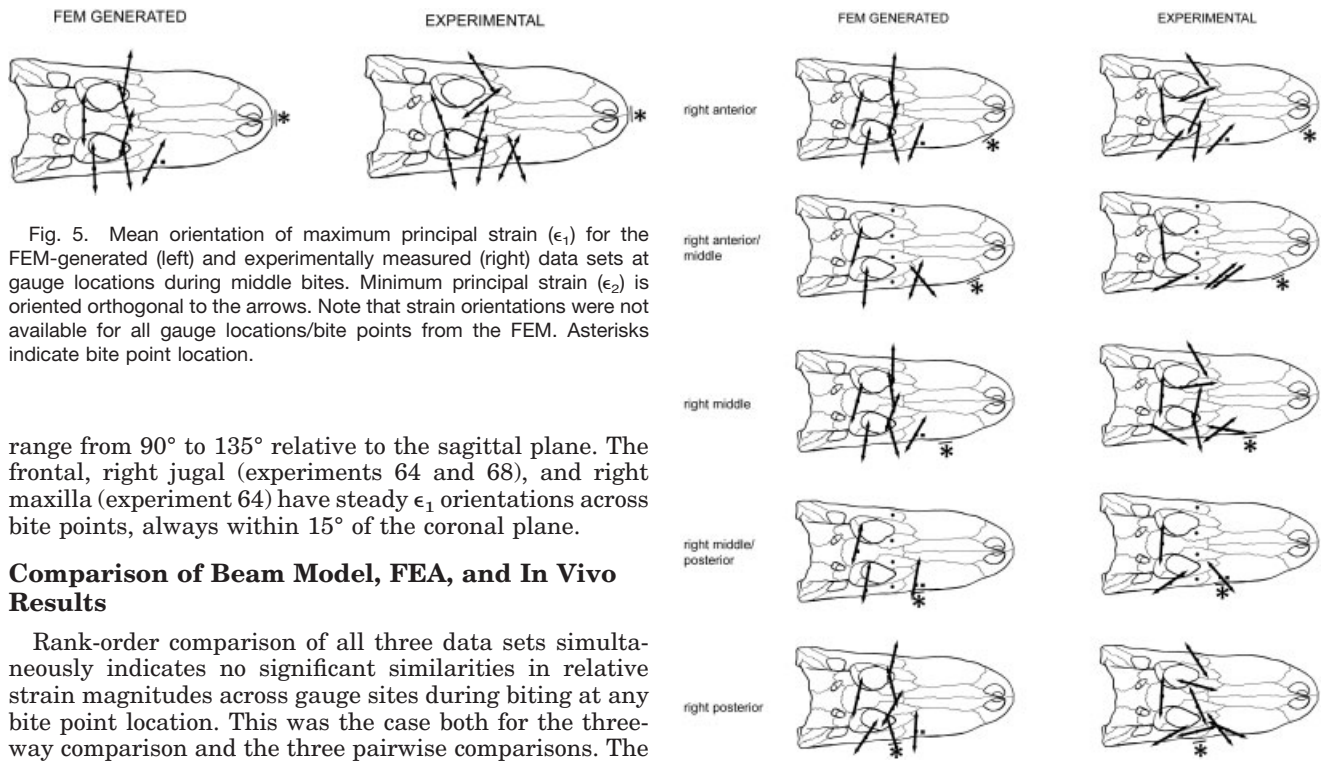
Fig. 5. Mean orientation of maximum principal strain (ϵ_1) for the FEM-generated (left) and experimentally measured (right) data sets at gauge locations during middle bites. Minimum principal strain (ϵ_2) is oriented orthogonal to the arrows. Note that strain orientations were not available for all gauge locations/bite points from the FEM. Asterisks indicate bite point location.

range from 90° to 135° relative to the sagittal plane. The frontal, right jugal (experiments 64 and 68), and right maxilla (experiment 64) have steady ϵ_1 orientations across bite points, always within 15° of the coronal plane.

Comparison of Beam Model, FEA, and In Vivo Results

Rank-order comparison of all three data sets simultaneously indicates no significant similarities in relative strain magnitudes across gauge sites during biting at any bite point location. This was the case both for the three-way comparison and the three pairwise comparisons. The lack of any statistically significant rank similarities makes it impossible to say definitively whether the FEM or beam model is a better predictor of strain magnitude similarity across in vivo gauge sites. Similarly, a graphic display of these data indicates almost no patterns of strain similarity across gauge sites (Fig. 8). Figure 8 displays strain magnitudes for the beam (top row), and the parasagittal component of strain magnitudes for the FEM (middle row), and experimental (bottom row) data sets for all bites, with gauge site locations listed across the x-axis from rostral (left) to caudal (right). The beam and FEM graphs show that compressive strain is predominant over tensile strain; the exceptions in the beam model are at the ventral-most sites, which most likely show tensile strain because the beam is modeled as fully elliptical rather than with a flattened ventral aspect. In contrast, the in vivo graphs show extensive tensile strains, even at extremely dorsal sites (prefrontal gauges). There is slight agreement among the data sets regarding where the highest magnitude strains are located, particularly between the FEM and in vivo data. Strains in the maxilla are typically compressive and small, while strains in the jugals (exper-

Fig. 6. Mean orientation of maximum principal strain (ϵ_1) for the FEM-generated (left) and experimentally measured (right) data sets at gauge locations during right anterior, right anterior/middle, right middle, right middle/posterior, and right posterior bites. See Figure 5 legend.

iment 68) are typically compressive and high. However, there is no statistical significance to this, and there are notable exceptions, such as the tensile strain in the jugals during posterior in vivo bites.

Comparison of FEA and In Vivo Results

Principal strain magnitudes. Mean principal strains (ϵ_1 and ϵ_2) are greater for the in vivo than for the finite-element model derived data in 111 of 132 cases (84%; Tables 3–5). When an FEM-derived principal strain is greater than the corresponding in vivo strain, it is almost always minimum principal (compressive) strain, and almost half of these cases are for a single gauge (frontal gauge; experiment 64). Mean FEM ϵ_1
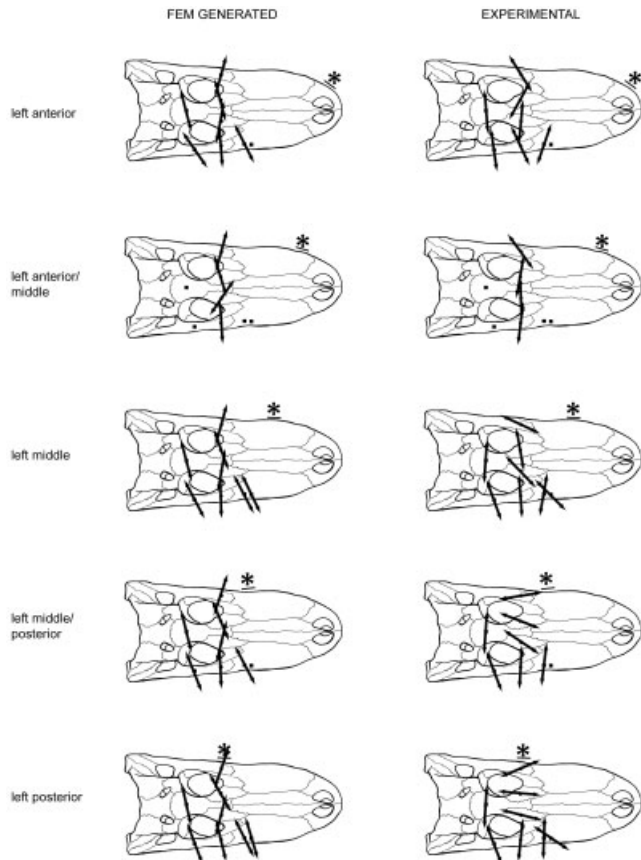
FEM GENERATED   EXPERIMENTAL

Fig. 7. Mean orientation of maximum principal strain (ϵ_1) for the FEM-generated (left) and experimentally measured (right) data sets at gauge locations during left anterior, left anterior/middle, left middle, left middle/posterior, and left posterior bites. See Figure 5 legend.

magnitude is 123 $\mu\epsilon$ (range, -151–721 $\mu\epsilon$) and mean in vivo ϵ_1 magnitude is 487 $\mu\epsilon$ (range, 5–1,746 $\mu\epsilon$). Mean FEM ϵ_2 magnitude is -306 $\mu\epsilon$ (range, -30 to $-1,305$ $\mu\epsilon$) and mean in vivo ϵ_2 magnitude is -582 $\mu\epsilon$ (range, 659 to $-2,286$ $\mu\epsilon$). The FEM and in vivo maximum principal strain magnitudes are not correlated either when grouped together or split into separate experiments (Fig. 9; all experiments: $r = 0.105$, NS; experiment 64: $r = 0.102$, NS; experiment 68: $r = 0.314$, NS; experiment 103: $r = -0.98$, NS).

Principal (ϵ_1) strain orientations. The difference between the model and experimental data is less notable for strain orientations then for strain magnitudes. The average difference between the model-derived and the in vivo ϵ_1 strain orientations for all bite locations and gauge sites is 33.4°, and when gauge sites are considered separately, this average difference ranges from 7° to 55° (Figs. 5–7, Tables 6–8). Additionally, model-derived and in vivo strain orientations have a tendency to be more similar at gauge sites that are located further away from the bite point location. For example, during left side biting at various bite point locations, ϵ_1 orientation at the FEM right jugal gauge site (experiment 64) differed from the in vivo data by an average of only 9°. However, during right

side bites, the FEM ϵ_1 orientations differ from the in vivo results by an average of 39° (Table 6). FEM vs. in vivo differences tend to be larger at more posterior bite point locations (7 of 13 gauge sites/bite sides follow this pattern). Model-derived ϵ_1 orientations from the frontal gauge have the lowest average difference from the in vivo data across bite points (7°; Table 6).

DISCUSSION
Beam Theory-Derived Strain Magnitudes

Strain due to bending. The cross-sectional geometry of a beam has a significant effect on the distribution of strain throughout it. Under pure bending, normal strain within a cross-section increases with distance from the neutral axis of bending (Fig. 4A). In addition, sections closer to the fixed end of the beam will experience higher normal strains at equivalent distances from the neutral axis. This pattern was not seen in our beam model data (Table 2) because we modeled each section as having a unique second moment of area and hence different distances to the gauge locations from the neutral axis.

Variation in compressive strain magnitude at the maxillary, prefrontal, and jugal sites is a function of the magnitude of the perpendicular distance from the neutral axis and the second moment of area. Not surprisingly, strains in our solid beam model are significantly lower (1–2 orders of magnitude) than those typically seen in limb bones (Biewener, 1990) or mandibles (Dechow and Hylander, 2000), which are generally either flat or have medullary cavities, resulting in lower second moments of area and consequently higher strains.

Strain due to torsion. In a beam with an elliptical cross-section loaded in pure torsion, the maximum shear stress and strain is expected to occur at a point on the surface of the beam that is closest to the twisting axis (Fig. 4B). Additionally, in cross-sectional view, shear stresses increase with the distance outward from the twisting axis (Hibbeler, 2000: p. 221). Unlike during bending, the distribution of shear stress will be the same at any cross-section in the beam, regardless of the distance between the cross-section and the fixed end of the beam.

Comparison of Models and In Vivo Data

As noted above, there were clear differences between the beam model, FE model, and the recorded in vivo strains, both with regard to the absolute strain magnitudes and the patterns of strain gradients across the skull. Low strains in the beam model were expected. There are several possible explanations why principal strain magnitudes were much higher in vivo than in the FEM. The most likely cause is that the scaling method used for constructing this model from a larger specimen (geometric similarity) resulted in thickened rostral bone relative to size for the scaled models, which would decrease principal strain values. In reality, it is expected that rostral bone thickness does not scale with isometry and therefore would be thinner than in the model. Two other possibilities for this discrepancy relate to the material properties of bone in the FEM. First, if an incorrect elastic modulus were used, this would not have much of an impact on stress magnitudes, but would greatly impact strain magnitudes (Daniel and McHenry, 2001). Second, during preliminary testing of the FEM, modeling the bone as isotropic resulted in lower stresses and presumably lower

TABLE 9. Descriptive statistics for shear (γ_{max}) strain values for in vivo experiment 64

Gauge location	Bite location		n	γ_{max} ($\mu\epsilon$)		
				Mean	SD	Max
Frontal	Midline		2	605	716	1,111
	Left	a	4	315	129	496
		m	9	1,076	508	1,778
		m/p	7	1,269	257	1,576
		p	7	893	182	1,187
	All left		27	966	447	
	Right	a	2	380	51	416
		a/m	4	858	468	1,321
		m	11	1,057	375	1,468
		m/p	7	810	249	1,140
		p	9	434	122	593
	All right		33	770	389	
	All bites		60	631	342	
Right jugal	Midline		2	201	209	349
	Left	a	4	161	27	198
		m	9	653	329	1,004
		m/p	7	862	143	989
		p	7	606	128	806
	All left		27	622	301	
	Right	a	2	337	36	362
		a/m	4	1,425	716	2,153
		m	11	3,037	1,250	4,973
		m/p	7	3,653	966	4,851
		p	9	2,528	659	3,341
	All right			2,670	1,272	
	All bites		60	1,698	1,409	
Right maxilla	Midline		2	470	550	858
	Left	a	4	170	87	287
		m	9	463	267	832
		m/p	7	490	134	662
		p	7	281	93	422
	All left		27	379	210	
	Right	a	2	440	4	442
		a/m	4	1,514	1,011	2,553
		m	11	2,564	1,089	4,269
		m/p	7	1,924	985	3,621
		p	9	458	272	1,021
	All right			1,598	1,209	
	All bites		60	1,031	1,078	

strains, and it is very likely that the crocodilian skull, like other vertebrate skulls, is generally orthotropic (Peterson and Dechow, 2003). Material testing of gauge sites will help to address these two issues.

Because in vivo and FEM loading is complex, it is difficult to determine why there was no similarity in rank-order patterns of strain magnitude between the three data sets. Incongruence between the models and the in vivo data may be attributable to a number of factors, such as local effects of muscles that were not accounted for in the FE or beam models, local effects of bite force, effects of sutures, or the presence of a complex, combined loading regime in vivo.

The strain orientations predicted by beam theory (Fig. 1) and the FEA and in vivo orientation values measured from the alligator rostum, jugals, and frontal bone (Figs. 5–7) allow evaluation of hypotheses that during midline (middle) biting, the snout can be modeled as a beam experiencing dorsally directed bending, and that during unilateral biting, the snout acts as an ellipsoid beam subjected to superimposed twisting and bending regimes.

During anterior midline bites, the strain orientations from both the FEM and in vivo strain gauges (Fig. 5) are indicative that the rostrum is acting as a cantilevered beam that is being bent dorsally concave (as in Fig. 1A). Although the FEM orientations are slightly more consistent with this hypothesis than in vivo orientations, this is not surprising considering that anterior midline bites during the in vivo experiments may have sometimes deviated slightly from the midline, creating torsional moments.

It is more difficult to assess whether unilateral biting causes the snout to act like a twisted beam because of the potentially confounding effects of the superimposed bending regime. However, if it is presumed that unilateral biting causes the working side to be twisted in a dorsal direction due to the dorsally directed bite force (Busbey, 1995; Preuschoft and Witzel, 2002), we should expect strain orientations to be approximately 45° during right side bites and −45° during left side bites (relative to the sagittal plane). The in vivo strain orientations generally confirm this hypothesis, especially when the animals bit at the right anterior, right anterior/middle, and left side bite point locations (Figs. 6 and 7).

FEM strain orientations confirmed the hypothesis of a combined loading in bending and torsion, although there was a noted asymmetry in the FEM results (Figs. 6 and 7).

TABLE 10. Descriptive statistics for shear (γ_{max}) strain values for in vivo experiment 68

Gauge location	Bite location		n	γ_{max} ($\mu\epsilon$) Mean	SD	Max
Right jugal	Midline		10	1,047	1,067	3,277
	Left	a	4	751	914	2,088
		a/m	3	1,411	995	2,043
		m	16	833	702	2,299
		m/p	13	870	608	1,806
		p	7	1,208	467	1,667
	All left		43	938	676	
	Right	a	5	1,733	859	2,772
		m	20	2,987	549	3,781
		m/p	1	1,099		1,099
		p	10	1,803	696	2,677
	All right		36	2,432	884	
	All bites		89	1,619	1,076	
Right prefrontal	Midline		10	809	853	2,826
	Left	a	4	468	386	1,015
		a/m	3	683	427	947
		m	10 (6)	226 (427)	173 (297)	776
		m/p	11 (2)	534 (442)	75 (4)	1,132
		p	7	762	366	1,150
	All left		43	468	377	
	Right	a	5	1,165	587	1,874
		m	17 (3)	2,157 (455)	582 (240)	2,784
		m/p	1	49		49
		p	6 (4)	668 (165)	84 (69)	789
	All right		36	1,349	937	
	All bites		89	869	816	
Left prefrontal	Midline		10	1,086	646	2,777
	Left	a	4	690	211	931
		a/m	3	1,179	682	1,913
		m	16	559	442	1,629
		m/p	13	987	804	2,210
		p	7	1,352	620	1,821
	All left		43	873	651	
	Right	a	5	1,862	672	2,435
		m	16 (4)	3,833 (2901)	482 (599)	4,434
		m/p	1	1,507		1,507
		p	10	2,315	917	3,445
	All right		36	2,970	1,053	
	All bites		89	1,828	1,353	
Left jugal	Midline		10	961	1,043	3,103
	Left	a	4	1,130	1,412	3,237
		a/m	3	2,177	1,551	3,307
		m	10 (6)	1,438 (654)	1,049 (361)	3,245
		m/p	11 (2)	1,829 (565)	1,130 (582)	3,572
		p	7	2,818	905	3,612
	All left		43	1,636	1,205	
	Right	a	5	498	400	1,174
		m	20	1,319	385	1,864
		m/p	1	1,432		1,432
		p	10	987	342	1,401
	All right		36	1,116	463	
	All bites		89	1,399	973	

Orientations during right side bite FEM loadings were less consistent with this loading regime than during left side bites. A possible explanation for these unexpected results is that most of the strain gauge sites were located on the right side of the skull, and the FEM may have exhibited unusual behavior when the bite point too closely approached the gauge site. This deviation of strain orientation from the expectation of a twisted ellipsoid beam during unilateral biting was also found in the in vivo results when the bite point was located adjacent to the gauge (e.g., Fig. 6, right posterior bites; Fig. 6, left middle/posterior, left posterior bites), lending credence to this hypothesis. In these cases, ϵ_1 is oriented in the sagittal plane and probably represents a local loading regime due to localized effects of bite force rather than a global one acting on the entire snout.

The relative invariance of principal strain orientations in the frontal gauge location, in both the FEM and the in vivo strain experiments, is notable. In all cases, this orientation is indicative of dorsal bending in the region be-

TABLE 11. Descriptive statistics for shear (γ_{max}) strain values for in vivo experiment 103

Gauge location	Bite location		n	γ_{max} ($\mu\epsilon$)		
				Mean	SD	Max
Right maxilla	Left	m	6	324	106	518
		p	5	254	129	453
	All left		11	292	117	518
	Right	a/m	4 (2)	2,382 (3,031)	540 (153)	3,139
		m	2	3,624	865	4,235
		p	5	3,943	208	4,160
	All right		13	3,273	796	4,235
	All bites		24	1,907	1,624	4,235

tween the orbits. We suggest that this similarity may indicate that the dorsal roof of the braincase is part of a functionally discrete region, distinct from more rostral areas of the cranium, and subject to different loading conditions. However, further testing is needed to confirm this hypothesis.

Beams (Greaves, 1985; Thomason, 1991; Weishampel, 1993; Covey and Greaves, 1994; Busbey, 1995) and finite-element analyses (Daniel and McHenry, 2001; Strait et al., 2003; Rayfield, 2005, this issue) have often been used to represent loading regimes within the vertebrate cranium theoretically. The results of this study indicate that neither simple beam theory nor a finite-element model is able to provide a completely accurate prediction of the nature of in vivo strain recorded from the alligator cranium. Specifically, the models were not able to represent absolute in vivo strain magnitudes or strain gradients accurately.

The poor correspondence between the *Alligator* FEA and in vivo strain data stands in stark contrast to the close correspondence in the studies of the macaque skull published elsewhere in this volume (Ross et al., 2005, this issue; Strait et al., 2005, this issue). These differing degrees of correspondence might be attributable to differences in modeling procedures. Most notably, the *Alligator* model used in this study was of relatively low resolution and so did not include the detailed geometry of the macaque model. Similarly, the material properties and muscle forces used in the macaque model are arguably more realistic than those used in the *Alligator* model.

We hypothesize that one significant difference between the two models lies in the relative importance of sutures in the biomechanical functioning of the two skulls. Numerous experimental studies have shown that sutures typically exhibit strain magnitudes that are an order of magnitude higher than those in the bones that they connect, and strains can be reduced or reoriented across sutures (Jaslow, 1990; Jaslow and Biewener, 1995; Rafferty and Herring, 1999; Herring and Teng, 2000; Metzger and Ross, 2001; Rafferty et al., 2003; Lieberman et al., 2004). The principal strain values recorded from the alligators in vivo are on average greater than those recorded from any other vertebrate cranial bones that have been extensively sampled (Hylander, 1979; Hylander and Johnson, 1992; Herring et al., 1996; Ross and Hylander, 1996; Hylander and Johnson, 1997; Herring and Teng, 2000; Ravosa et al., 2000; Ross, 2001; Thomason et al., 2001; Lieberman et al., 2004; Ross and Metzger, 2004). If sutural strain increases as a function of bone strain, the very high bone strain magnitudes recorded in this study predict extremely high

sutural strains, suggesting that sutural morphology might be of great importance in the functioning of the *Alligator* skull, as it appears to have been in dinosaurs (Rayfield, 2005, this issue) and at least some mammals (Herring and Teng, 2000).

The results of this study should serve as a caveat against the exclusive use of FEA or beam modeling techniques to demonstrate loading patterns in a complex skeletal structure such as the cranium, which is subjected to unpredictable and highly dynamic forces. However, even using relatively low-resolution finite-element and beam models, we can reproduce the basic strain orientations that were seen in vivo, indicating that both of these modeling techniques have the utility of serving as a first-pass approximation of the in vivo loading conditions. While beam and FE analyses are suitable first-pass estimations for strain orientations, we advocate that whenever possible, hypotheses related to loading in the vertebrate cranium should be supported with either in vivo or in vitro strain data.

Loading Regimes in Crocodilian Skull

Although the principal strain orientations recorded in vivo are not precisely those predicted by either the beam models or the FEA, the strain orientation data strongly suggest that the snout is bent upward and twisted during biting. If this hypothesis is correct, then, as suggested by Busbey (1995), the cross-sectional profile of the *Alligator* rostrum is not optimized for resisting the loading regimes to which it is subjected during feeding. This is even more remarkable, considering the high principal strain magnitudes recorded from the *Alligator* skull in vivo (Ross and Metzger, 2004) compared to the relatively low strain magnitudes recorded from the *Alligator* postcranium (Blob and Biewener, 1999). Whether the cranial/postcranial differences reflect differing optimality criteria in the cranial versus the postcranial skeleton, differing material properties, or differing success in eliciting vigorous locomotor versus biting behavior (Ross and Metzger, 2005), it is clear that explanations for the cross-sectional geometry of the alligator snout must invoke a function other than dissipating feeding forces. One possibility is Busbey's (1995) suggestion that the platyrostral geometry of the crocodilian snout is optimized for lateral snapping movements used in the capture of prey in an aquatic environment. The consequent decreased ability of the snout to resist dorsoventral bending is compensated for by the evolution of a hard palate and decreased resistance to torsion is compensated for by scarf joints at the sutures (Busbey, 1995). If this hypothesis is correct, then the *Alligator* snout is sim-
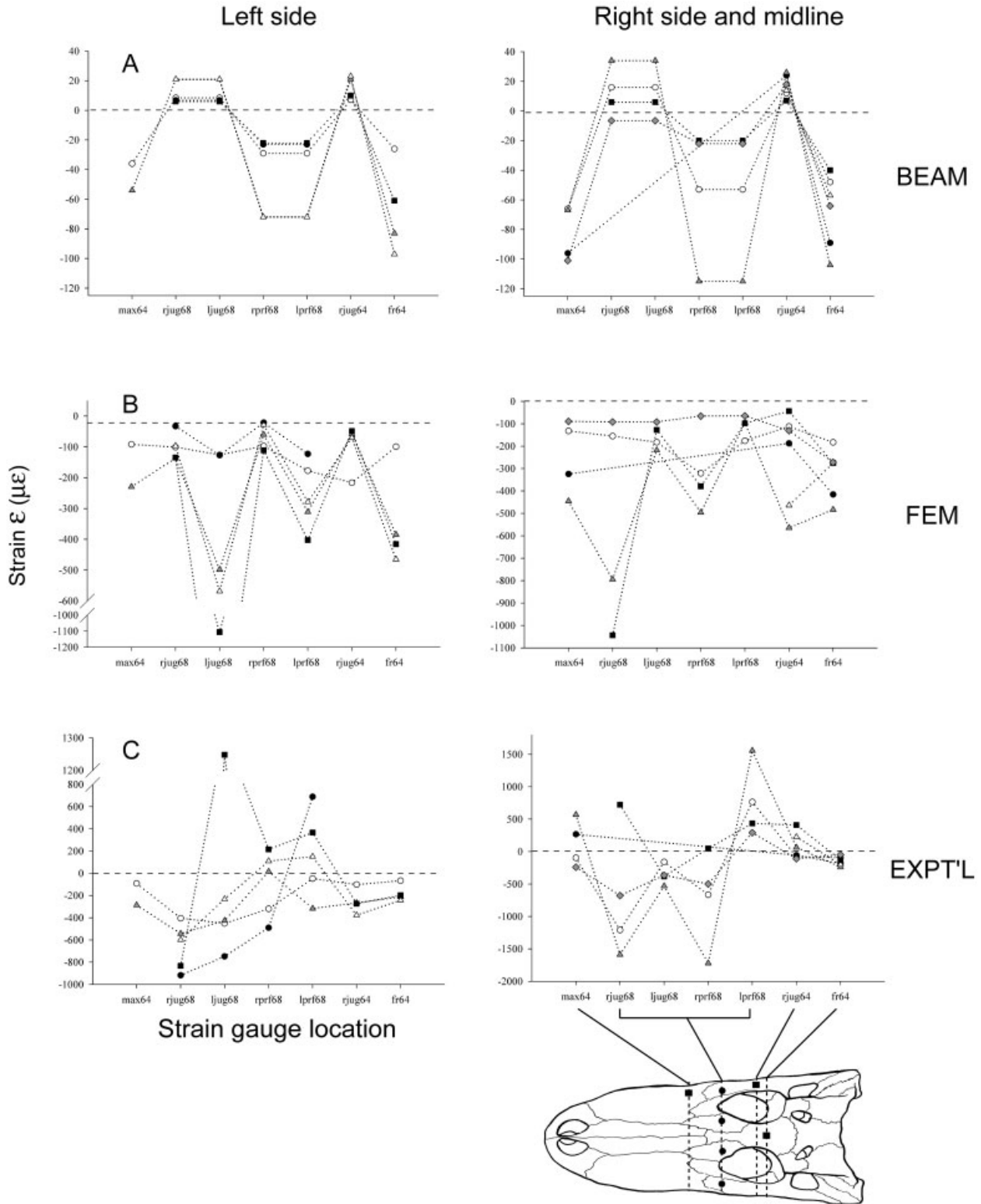
Fig. 8. Component of strain magnitudes (με) parallel to the parasagittal plane for the beam (top row), FEM (middle row), and experimental (bottom row) data sets. Left side bites are in the left column and midline and right side bites are in the right column. Within each smaller plot, values are plotted by strain gauge site, progressing from rostral sites to caudal sites (left to right). Multiple lines within each smaller graph indicate different bite point locations. Gray diamonds, midline bites; open circles, anterior bites; black circles, anterior/middle bites; gray triangles, middle bites; open triangles, middle/posterior bites; black squares, posterior bites.
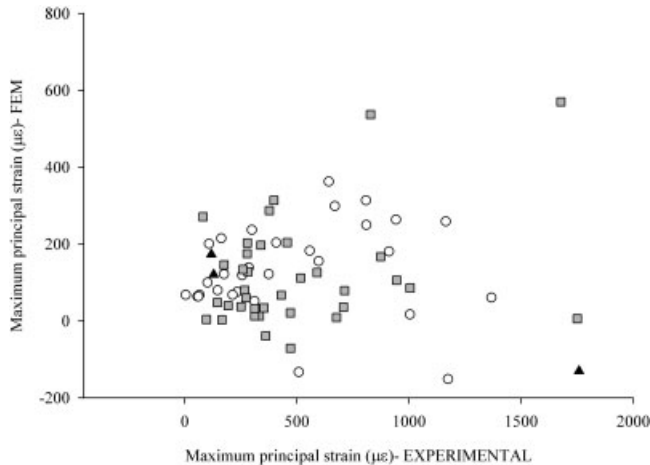
Fig. 9. Bivariate plot of experimentally recorded maximum principal strain vs. model-derived maximum principal strain magnitudes. Each point represents the average of all bites from a single bite point location for a particular gauge. Gray squares, experiment 64; open circles, experiment 68; black triangles, experiment 103.

ilar to various parts of the primate skull in that the function of dissipating feeding forces appears to have exerted little constraint on the geometry of the cranium (Hylander et al., 1991; Ravosa et al., 2000; Ross, 2001).

ACKNOWLEDGMENTS

LITERATURE CITED

Biewener AA. 1990. Biomechanics of mammalian terrestrial locomotion. Science 250:1097–1103.

Biewener AA. 1992. Biomechanics-structures and systems: a practical approach. Oxford: Oxford University Press.

Blob RW, Biewener AA. 1999. *In vivo* locomotor strain in the hindlimb bones of *Alligator mississippiensis* and *Iguana iguana*: implications for the evolution of limb bone safety factor and non-sprawling posture. J Exp Biol 202:1023–1046.

Brochu CA, Rowe T, Kishi K, Merck JW Jr, Colbert MW, Saglamer E, Warren S. 1998. University of Texas Digimorph. TX: University of Texas, Austin, TX.

Busbey AB. 1989. Form and function of the feeding apparatus of *Alligator mississippiensis*. J Morphol 202:99–127.

Busbey AB. 1995. The structural consequences of skull flattening in crocodilians. In: Thomason JJ, editor. Functional morphology in vertebrate paleontology. Cambridge: Cambridge University Press. p 173–192.

Cleuren J, De Vree, F. 2000. Feeding in crocodilians. In: Schwenk K, editor. Feeding: form, function and evolution in tetrapod vertebrates. San Diego, CA: Academic Press. p 337–358.

Covey DSJ, Greaves WS. 1994. Jaw dimensions and torsion resistance during canine biting in the Carnivora. Can J Zool 72:1055–1060.

Daniel WJT, McHenry C. 2001. Bite force to skull stress correlation: modeling the skull of *Alligator mississippiensis*. In: Grigg GC, Seebacher F, Franklin CE, editors. Crocodilian biology and evolution. New South Wales, Australia: Surrey Beatty & Sons. p 135–143.

Dechow PC, Hylander WL. 2000. Elastic properties and masticatory bone stress in the macaque mandible. Am J Phys Anthropol 112:553–574.

Endo B. 1966. A biomechanical study of the human facial skeleton by means of strain-sensitive lacquer. Okajimas Folia Anat Jpn 42:205–217.

Ferguson MWJ. 1981. The value of the American alligator (*Alligator mississippiensis*) as a model for research in craniofacial development: review. J Craniofac Genet Dev Biol 1:123–144.

Greaves WS. 1985. The mammalian postorbital bar as a torsion-resisting helical strut. J Zool Soc 207:125–136.

Gross TS, Edwards JL, McLeod KJ, Rubin CT. 1997. Strain gradients correlate with sites of periosteal bone formation. J Bone Miner Res 12:982–988.

Gross TS, Srinivasan S, Liu CC, Clemens TL, Bain SD. 2002. Noninvasive loading on the murine tibia: an in vivo model for the study of mechanotransduction. J Bone Miner Res 17:493–501.

Gupta S, van der Helm FCT, Sterk JC, Van Keulen F, Kaptein BL. 2004. Development and experimental validation of a three-dimensional finite element model of the human scapula. J Engineer Med 218:127–142.

Herrel, A, Van Damme R, Vanhooydonck B, De Vree F. 2001. The implications of bite performance for diet in two species of lacertid lizards. Can J Zool 79:662–670.

Herring SW, Teng S, Huang X, Mucci R, Freeman J. 1996. Patterns of bone strain in the zygomatic arch. Anat Rec 246:446–457.

Herring S, Teng S. 2000. Strain in the braincase and its sutures during function. Am J Phys Anthropol 112:575–593.

Hibbeler RC. 2000. Mechanics of materials, 4th ed. Upper Saddle River, NJ: Prentice Hall.

Hylander W. 1979. Mandibular function in *Galago crassicaudatus* and *Macaca fascicularis*: an in vivo approach to stress analysis of the mandible. J Morphol 159:253–296.

Hylander WL, Picq PG, Johnson KR. 1991. Masticatory-stress hypotheses and the supraorbital region of primates. Am J Phys Anthropol 86:1–36.

Hylander WL, Johnson KR. 1992. Strain gradients in the craniofacial region of primates. In: Davidovich Z, editor. The biological mechanisms of tooth movement and craniofacial adaptation. Columbus, OH: Ohio State University. p 559–569.

Hylander WL, Johnson KR. 1997. In vivo bone strain patterns in the zygomatic arch of macaques and the significance of these patterns for functional interpretations of craniofacial form. Am J Phys Anthropol 102:203–232.

Jaslow CR. 1990. Mechanical properties of cranial sutures. J Biomech 23:313–321.

Jaslow CR, Biewener AA. 1995. Strain patterns in the horncores, cranial bones and sutures of goats (*Capra hircus*) during impact loading. J Zool 235:193–210.

Kotha SP, Hsieh Y-F, Strigel RM, Müller R, Silva MJ. 2004. Experimental and finite element analysis of the rat ulnar loading model-correlations between strain and bone formation following fatigue loading. J Biomech 37:541–548.

Langston W Jr. 1973. The crocodilian skull in historical perspective. In: Gans C, editor. Biology of the reptilia, vol. 4, morphology D. New York: Academic Press. p 263–284.

Lieberman DE, Krovitz GE, Yates FW, Devlin M, St. Claire M. 2004. Effects of food processing on masticatory strain and craniofacial growth in a retrognathic face. J Hum Evol 46:655–677.

Metzger K, Ross C. 2001. Strain patterns in the lower jaw of the caiman (*Caiman crocodilus*): implications for the function and evolution of the intramandibular joint in archosaurs. J Morphol 248:261–262.

Metzger KA, Ross CF, Spencer MA. 2003. Does the constrained lever model describe an optimality criterion in crocodilian jaw mechan-

ics? SICB 2004 New Orleans: Integrative and Comparative Biology 43:825.

Peterson J, Dechow PC. 2003. Material properties of the human cranial vault and zygoma. Anat Rec 274A:785–797.

Preuschoft H, Demes B, Meyer M, Bar HF. 1983. The biomechanical principles realised in the upper jaw of long-snouted primates. In: Else JG, Lee PC, editors. Primate evolution: proceedings of the 10th Congress of the International Primatological Society, vol. 1. Cambridge: Cambridge University Press. p 249–264.

Preuschoft H, Demes B, Meier M, Bar HF. 1986. Les principes mécaniques réalisés dans la mâchoire supérieure des vertèbrés a museau long. In: Sakka M, editor. Définition et origines de l'homme: table ronde internationale no 3 CNRS. Paris: Editions de CNRS. p 177–198.

Preuschoft H, Witzel U. 2002. Biomechanical investigations on the skulls of reptiles and mammals. Senckenbergiana Lethaea 82:207–222.

Rafferty K, Herring S. 1999. Craniofacial sutures: morphology, growth, and in vivo masticatory strains. J Morphol 242:167–179.

Rafferty KL, Herring SW, Marshall CD. 2003. Biomechanics of the rostrum and the role of facial sutures. J Morphol 257:33–44.

Ravosa M, Johnson K, Hylander W. 2000. Strain in the galago facial skeleton. J Morphol 245:51–66.

Rayfield EJ. 2005. Using finite element analysis to investigate suture morphology—a case study using large, carnivorous dinosaurs. Anat Rec 283A:349–365.

Ross CF, Hylander WL. 1996. In vivo and in vitro bone strain in the owl monkey circumorbital region and the function of the postorbital septum. Am J Phys Anthropol 101:183–215.

Ross CF. 2001. In vivo function of the craniofacial haft: the interorbital "pillar." Am J Phys Anthropol 116:108–139.

Ross CF, Metzger KA. 2004. Bone strain gradients and optimization in vertebrate skulls. Ann Anat 186:387–396.

Ross CF, Patel BA, Slice DE, Strait DS, Dechow PC, Richmond BG, Spencer MA. 2005. Modeling masticatory muscle force in finite-element analysis: sensitivity analysis using principal coordinates analysis. Anat Rec 283A:288–299.

Russell AP, Thomason JJ. 1993. Mechanical analysis of the mammalian head skeleton. In: Hanken J, Hall BK, editors. The skull, vol. 3, functional and evolutionary mechanisms. Chicago: Chicago University Press. p 345–383.

Sinclair AG, Alexander RM. 1987. Estimates of forces exerted by the jaw muscles of some reptiles. J Zool 213:107–115.

Strait DS, Dechow PC, Richmond BG, Ross CF, Spencer MA. 2003. Finite element analysis applied to masticatory biomechanics. Am J Phys Anthropol S36:202.

Strait DS, Wang O, Dechow PC, Ross CF, Richmond BG, Spencer MA, Patel BA. 2005. Modeling elastic properties in finite-element analysis: How much precision is needed to produce an accurate model? Anat Rec 283A:275–287.

Thomason JJ, Russell AP. 1986. Mechanical factors in the evolution of the mammalian secondary palate: a theoretical analysis. J Morphol 189:199–213.

Thomason JJ. 1991. Cranial strength in relation to estimated biting forces in some mammals. Can J Zool 69:2326–2337.

Thomason JJ, Grovum LE, Deswysen AG, Bignell WW. 2001. In vivo surface strain and stereology of the frontal and maxillary bones of sheep: implications for the structural design of the mammalian skull. Anat Rec 264:325–338.

Weishampel DB. 1993. Beams and machines: modeling approaches to the analysis of skull form and function. In: Hanken J, Hall BK, editors. The skull, vol. 3, functional and evolutionary mechanisms. Chicago: Chicago University Press. p 303–344.